V European Conference on Computational Fluid Dynamics
ECCOMAS CFD 2010
J. C. F. Pereira and A. Sequeira (Eds)
Lisbon, Portugal,14-17 June 2010

RECENT ADVANCES ON THE IMMERSED STRUCTURAL POTENTIAL METHOD FOR FLUID-STRUCTURE INTERACTION HAEMODYNAMIC APPLICATIONS.

Antonio J. Gil*, Aurelio Arranz Carreño*, J. Bonet* and O. Hassan*

*School of Engineering, Swansea University,
Singleton Park, SA2 8PP, UK
e-mail: {a.j.gil, a.arranz-carreno, j.bonet, o.hassan}@swansea.ac.uk

Key words: fluid-structure interaction, immersed boundary method, haemodynamics, heart valves

Abstract. *In this paper, recent advances on the Immersed Structural Potential Method (ISPM)[1] are presented. This methodology, based on the original Immersed Boundary Method[2], was introduced with the purpose of modelling Fluid-Structure Interaction (FSI) haemodynamic problems. The ISPM presents an alternative approach to compute the equivalent fluid-structure interaction forces at the fluid mesh, accounts for a sophisticated viscoelastic fibre-reinforced constitutive model to better describe the mechanics of cardiovascular tissues and utilises a novel time-integration methodology for the computation of the deformation gradient tensor which ensures compliance with the incompressibility constraint. Comparison of the ISPM with alternative existing immersed methodologies will be presented as well as various idealised cardiovascular numerical examples in order to demonstrate the robustness and applicability of this numerical technique.*

1 INTRODUCTION

The Immersed Boundary Method (IBM) was initially introduced[2] with the purpose of studying flow patterns around heart valves. The defining characteristic of "immersed methods" is the numerical treatment of any solid structure within the fluid as a field of body forces via convolution with smoothed approximations (kernels) of the Dirac delta distribution. Immersed techniques posses many attractive features, particularly when large deformation of thin structures in three dimensions is considered. Unfortunately, the original IBM method is restricted to massless fibre-like (one dimensional) structures immersed within the fluid and the discrete convolution with these kernels induces diffusive effects at the solid boundaries.

Some of the extensions of the original IBM, such as the EIBM-IFEM[3], have emerged in order to palliate the aforementioned limitations. These methodologies rely on the modelling of the immersed solid structure as a continuum spatially discretised by means

of an embedded Finite Element (F.E.) space. The deformation gradient tensor $\boldsymbol{F}$ is interpolated within the immersed continuum by using standard space-varying F.E. shape functions. Equivalent internal forces are computed at the nodes of the F.E. mesh after suitable numerical integration of the stress tensor evaluated at Gauss points. The equivalent nodal forces are then spread back to the Eulerian fluid domain. One disadvantage of this methodology is the non-satisfaction of the incompressibility constraint with negative implications in long term numerical simulations.

The Immersed Structural Potential Method (ISPM)[1] was introduced as an improvement to existing immersed methodologies. In this technique, the structure is modelled as a potential energy functional completely immersed within the surrounding viscous fluid, in such a way that the velocity field at any location within the structure domain is obtained by means of interpolating kernel functions constructed on the Eulerian fluid mesh. Hence, the structure is treated as a collection of integration points exclusively transported by the fluid. Both interpolation and spreading operations are greatly improved by interpolating in a similar fashion to the Material Point Method[4, 5], that is, the velocity field and the spatial velocity gradient tensor are sampled directly at integration points within the structure domain and the structural stresses are directly integrated back to the fluid fluid. Computational time as well as diffusion errors at interfaces are reduced, as no interpolation/spreading is carried out within the structure domain, in contrast with existing immersed methodologies.

The main objective of this article is to review the ISPM formulation, highlighting its advantages and displaying some comparative results with existing immersed methodologies. The paper is broken-down as follows. Section 2 describes the governing equations presented according to an integral conservation law formulation. The equations are particularised within the framework of a low order Finite Volume staggered method. Section 3 describes in detail the immersed methodology employed in order to evaluate the forcing term required when resolving the Navier-Stokes equations. Section 4 summarises the ISPM algorithm and displays its main differences with respect to existing immersed methodologies. Finally, section 5 presents some numerical results before some concluding remarks are drawn down.

2 GOVERNING EQUATIONS.

Let us consider the motion of a continuum defined by means of a mapping $\boldsymbol{\phi}$ established between a reference or material configuration $\boldsymbol{X} \in \Omega_0$ and a spatial or current configuration $\boldsymbol{x} \in \Omega$ at time t, namely $\boldsymbol{x}(t) = \boldsymbol{\phi}(\boldsymbol{X}, t)$. The deformation gradient tensor $\boldsymbol{F}$ is defined as the material gradient of the spatial position as:

$$\boldsymbol{F} = \nabla_0 \boldsymbol{x} = \frac{\partial \boldsymbol{x}}{\partial \boldsymbol{X}}, \quad J = \det \boldsymbol{F} \tag{1}$$

where J is the jacobian of the transformation. In addition, the velocity $\boldsymbol{u} = [u, v]^{\mathrm{T}}$ of the continuum is computed as $\boldsymbol{u}(\boldsymbol{X}, t) = \frac{\partial \boldsymbol{x}}{\partial t}$. The conservation of linear momentum for an

arbitrary spatial volume Ω is expressed in integral form as:

$$\frac{D}{Dt}\int_\Omega \rho\boldsymbol{u}\, dv = \int_\Omega \boldsymbol{g}\, dv + \int_{\partial\Omega} \boldsymbol{t}\, da \tag{2}$$

where $\boldsymbol{g}$ denotes an external volume force field per unit of volume and $\boldsymbol{t} = \boldsymbol{\sigma}\boldsymbol{n}$ is the traction vector associated to the Cauchy stress tensor $\boldsymbol{\sigma}$ and an element of area da in the boundary of the current configuration $\partial\Omega$ with outward unit normal $\boldsymbol{n}$. Decomposition of the stress tensor $\boldsymbol{\sigma}$ into its volumetric $-p\boldsymbol{I}$ and deviatoric $\boldsymbol{\sigma}'$ components renders:

$$\frac{D}{Dt}\int_\Omega \rho\boldsymbol{u}\, dv = \int_\Omega \boldsymbol{g}\, dv - \int_{\partial\Omega} p\boldsymbol{n}\, da + \int_{\partial\Omega} \boldsymbol{\sigma}'\boldsymbol{n}\, da \tag{3}$$

In addition, application of the Reynolds' transport theorem (Lie derivative) and the Gauss divergence theorem on the first term of the above equation (3) yields:

$$\int_\Omega \frac{\partial}{\partial t}(\rho\boldsymbol{u})\; dv + \int_{\partial\Omega} (\rho\boldsymbol{u}\otimes\boldsymbol{u})\cdot\boldsymbol{n}\, da = \int_\Omega \boldsymbol{g}\, dv - \int_{\partial\Omega} p\boldsymbol{n}\, da + \int_{\partial\Omega} \boldsymbol{\sigma}'\boldsymbol{n}\, da \tag{4}$$

In the case of a Newtonian viscous continuum, the deviatoric Cauchy stress tensor $\boldsymbol{\sigma}'$ can be expressed as:

$$\boldsymbol{\sigma}' = 2\mu\left(\boldsymbol{d} - \frac{1}{3}I_{\boldsymbol{d}}\boldsymbol{I}\right); \qquad I_{\boldsymbol{d}} = \mathrm{tr}\boldsymbol{d}; \qquad \boldsymbol{d} = \frac{1}{2}\left(\boldsymbol{l} + \boldsymbol{l}^{\mathrm{T}}\right) \tag{5}$$

where $\boldsymbol{d}$ is the strain rate tensor or rate of deformation tensor obtained as the symmetric part of the spatial velocity gradient tensor $\boldsymbol{l} = \boldsymbol{\nabla}\boldsymbol{u}$ and μ is the dynamic viscosity constant.

For an incompressible continuum, where the velocity field must be solenoidal $\boldsymbol{\nabla}\cdot\boldsymbol{u} = 0$, the above equation (4) is simplified to:

$$\int_\Omega \frac{\partial}{\partial t}(\rho\boldsymbol{u})\; dv + \int_{\partial\Omega} (\rho\boldsymbol{u}\otimes\boldsymbol{u} + p\boldsymbol{I} - \mu\boldsymbol{\nabla}\boldsymbol{u})\cdot\boldsymbol{n}\, da = \int_\Omega \boldsymbol{g}\, dv \tag{6}$$

which represents the conservation of linear momentum for an incompressible Newtonian viscous continuum in an integral format. Within the framework of low order Finite Volume schemes, Ω can be regarded as a control volume where above vector equation (6) can be re-interpreted according to an Eulerian variational formulation as the following weak form:

$$\delta\boldsymbol{W}^{\Omega}(\boldsymbol{\phi},\delta\boldsymbol{u}) = \delta\boldsymbol{W}^{\Omega}_{iner}(\boldsymbol{\phi},\delta\boldsymbol{u}) + \delta\boldsymbol{W}^{\Omega}_{int}(\boldsymbol{\phi},\delta\boldsymbol{u}) - \delta\boldsymbol{W}^{\Omega}_{ext}(\boldsymbol{\phi},\delta\boldsymbol{u}) = 0 \tag{7}$$

$$\delta\boldsymbol{W}^{\Omega}_{iner} = \int_\Omega \delta\boldsymbol{u}\cdot\frac{\partial}{\partial t}(\rho\boldsymbol{u})\; dv + \int_{\partial\Omega} \delta\boldsymbol{u}\cdot(\rho\boldsymbol{u}\otimes\boldsymbol{u})\cdot\boldsymbol{n}\, da \tag{8}$$

$$\delta\boldsymbol{W}^{\Omega}_{int}(\boldsymbol{\phi},\delta\boldsymbol{u}) = \int_{\partial\Omega} \delta\boldsymbol{u}\cdot(p\boldsymbol{I} - \mu\boldsymbol{\nabla}\boldsymbol{u})\cdot\boldsymbol{n}\, da \tag{9}$$

$$\delta\boldsymbol{W}^{\Omega}_{ext}(\boldsymbol{\phi},\delta\boldsymbol{u}) = \int_\Omega \delta\boldsymbol{u}\cdot\boldsymbol{g}\, dv \tag{10}$$

where $\delta \boldsymbol{u} = [\delta u, \delta v]^{\mathrm{T}}$ is an arbitrary piecewise constant virtual velocity field with support $\overline{\Omega} = \Omega \bigcup \partial\Omega$. Particularising for the case of a uniformly spaced Cartesian staggered mesh, let $\Omega_{u^{A_x}}$ and $\Omega_{v^{A_y}}$ be the control volumes associated with the Cartesian components of the velocity u^{A_x} and v^{A_y}, respectively, with an arrangement similar to that of a Marker And Cell (MAC) grid[6]. Here, A_x and A_y denote fluid cell edges perpendicular to the ox and oy Cartesian axes, respectively, and u^{A_x} and v^{A_y} their corresponding edge velocities, for which the above weak form (7) can be split into:

$$\delta W^{\Omega_{u^{A_x}}}\left(\boldsymbol{\phi}, \delta u^{A_x}\right) = \delta u^{A_x}\left[\int_{\Omega_{u^{A_x}}} \frac{\partial}{\partial t}\left(\rho u\right)\, dv + \int_{\partial\Omega_{u^{A_x}}} \boldsymbol{\mathcal{F}}_u \cdot \boldsymbol{n}\, da - \int_{\Omega_{u^{A_x}}} \boldsymbol{g}\cdot\boldsymbol{e}_x\, dv\right] \tag{11}$$

$$\delta W^{\Omega_{v^{A_y}}}\left(\boldsymbol{\phi}, \delta v^{A_y}\right) = \delta v^{A_y}\left[\int_{\Omega_{v^{A_y}}} \frac{\partial}{\partial t}\left(\rho v\right)\, dv + \int_{\partial\Omega_{v^{A_y}}} \boldsymbol{\mathcal{F}}_v \cdot \boldsymbol{n}\, da - \int_{\Omega_{v^{A_y}}} \boldsymbol{g}\cdot\boldsymbol{e}_y\, dv\right] \tag{12}$$

where $\{\boldsymbol{e}_x, \boldsymbol{e}_y\}$ is the standard Cartesian basis. Equations (11-12) represent the conservation of linear momentum variables ρu and ρv in an variational integral form with $\boldsymbol{\mathcal{F}}_u$ and $\boldsymbol{\mathcal{F}}_v$ their corresponding interface fluxes, namely:

$$\boldsymbol{\mathcal{F}}_u = \rho u \boldsymbol{u} + p\boldsymbol{e}_x - \mu\boldsymbol{\nabla} u, \qquad \boldsymbol{\mathcal{F}}_v = \rho v \boldsymbol{u} + p\boldsymbol{e}_y - \mu\boldsymbol{\nabla} v \tag{13}$$

The terms in above equations (11-12) can be approximated following a standard low order Finite Volume procedure for a staggered Cartesian grid with spacing Δx and Δy . Specifically, volume integrals $\int_\Omega dv$ are evaluated as:

$$\int_{\Omega_{u^{A_x}}} \frac{\partial}{\partial t}\left(\rho u\right)\, dv \simeq \Omega_{u^{A_x}} \frac{\Delta(\rho u^{A_x})}{\Delta t} \tag{14}$$

$$\int_{\Omega_{v^{A_y}}} \frac{\partial}{\partial t}\left(\rho v\right)\, dv \simeq \Omega_{v^{A_y}} \frac{\Delta(\rho v^{A_y})}{\Delta t} \tag{15}$$

being $\Omega_{u^{A_x}} = \Omega_{v^{A_y}} = \Delta x \Delta y$ the volume of a general control volume in the Cartesian grid and,

$$\int_{\Omega_{u^{A_x}}} \boldsymbol{g}\cdot\boldsymbol{e}_x\, dv \simeq \Omega_{u^{A_x}} g_x^{A_x} \tag{16}$$

$$\int_{\Omega_{v^{A_y}}} \boldsymbol{g}\cdot\boldsymbol{e}_y\, dv \simeq \Omega_{v^{A_y}} g_y^{A_y} \tag{17}$$

where $g_x^{A_x}$ and $g_y^{A_y}$ are the external forces per unit of volume allocated to control volumes $\Omega_{u^{A_x}}$ and $\Omega_{v^{A_y}}$, respectively. Similarly, the boundary integrals $\int_{\partial\Omega} da$ are evaluated after suitable numerical definition of approximate Riemann interface fluxes in order to

guarantee the stability of the scheme, namely $\boldsymbol{\mathcal{F}}_u^{num}$ and $\boldsymbol{\mathcal{F}}_v^{num}$. The pressure and viscous components of $\boldsymbol{\mathcal{F}}_u^{num}$ and $\boldsymbol{\mathcal{F}}_v^{num}$ are obtained following a standard central difference approach which yields,

$$\int_{\partial\Omega_{_{u^{A_x}}}} p\boldsymbol{e}_x \cdot \boldsymbol{n}\, da \simeq \Delta y \left(p_E^{A_x} - p_W^{A_x}\right) \tag{18}$$

$$\int_{\partial\Omega_{_{v^{A_y}}}} p\boldsymbol{e}_y \cdot \boldsymbol{n}\, da \simeq \Delta x \left(p_N^{A_y} - p_S^{A_y}\right) \tag{19}$$

and,

$$\int_{\partial\Omega_{_{u^{A_x}}}} \boldsymbol{\nabla} u \cdot \boldsymbol{n}\, da \simeq \Delta y \left(\frac{u_E^{A_x} - u^{A_x}}{\Delta x} - \frac{u^{A_x} - u_W^{A_x}}{\Delta x}\right) + \Delta x \left(\frac{u_N^{A_x} - u^{A_x}}{\Delta y} - \frac{u^{A_x} - u_S^{A_x}}{\Delta y}\right) \tag{20}$$

$$\int_{\partial\Omega_{_{v^{A_y}}}} \boldsymbol{\nabla} v \cdot \boldsymbol{n}\, da \simeq \Delta y \left(\frac{v_E^{A_y} - v^{A_y}}{\Delta x} - \frac{v^{A_y} - v_W^{A_y}}{\Delta x}\right) + \Delta x \left(\frac{v_N^{A_y} - v^{A_y}}{\Delta y} - \frac{v^{A_y} - v_S^{A_y}}{\Delta y}\right) \tag{21}$$

Finally, the convective components of the numerical fluxes, that is $\rho u\boldsymbol{u}$ and $\rho v\boldsymbol{u}$, are obtained using a stabilised convective approximation, such as QUICK, SMART, VONOS or HLPA, which minimise numerical diffusion, avoid the creation of spurious oscillations and reduce the total variation of the solution by accounting for the transportive nature of the fluid.

3 Immersed structural potential.

Let us consider an incompressible deformable solid fully immersed within the surrounding incompressible viscous fluid. Following a numerical immersed strategy, the solid can be modelled as a Helmholtz's free energy functional whose spatial gradient defines a fluid-structure interaction force field which is regarded as an external force field by the background viscous fluid. In addition, if the background fluid is incompressible and ensuring that the numerical scheme used to solve the background fluid is free-divergence velocity preserving, only the deviatoric component of the solid stress will need to be taken into consideration. Hence, an equivalent homogeneous (distortional) component of the solid energy functional $\widehat{\Psi}^s$ will be defined in terms of the isochoric component of the strain.

For spatial semi-discretisation purposes, the solid domain is modelled in a Lagrangian manner as a collection of integration points a_p immersed within the fluid, moving from an initial position $\boldsymbol{X}^{a_p}$ to the spatial position $\boldsymbol{x}^{a_p}$ at time instant t, through the deformation gradient tensor $\boldsymbol{F}$ defined by the motion of the surrounding continuum (i.e. non-slip condition). To describe the constitutive behaviour of the structure and within the context of hyperelasticity, a potential energy functional Π^s is the introduced,

$$\Pi^s(\boldsymbol{\phi}) = \int_{\Omega_0^s} \widehat{\Psi}^s\left(\boldsymbol{\phi}\right) dV \simeq \sum_{a_p} \widehat{\Psi}^s\left(\boldsymbol{\phi}^{a_p}\right) W^{a_p} \tag{22}$$

where $\widehat{\Psi}^s$ is the stored strain energy density functional per unit of undeformed volume Ω_0^s and W^{a_p} is the material or Lagrangian weight associated with a structure integration point a_p. With the purpose of distinguishing the surrounding fluid phase from the immersed solid phase, a superindex $(.)^s$ will be employed when referring to the latter. The velocity of the deformable immersed solid can be obtained after suitable definition of an interpolation operator which enables to transfer information from the background Eulerian fluid to the Lagrangian solid. Specifically, the velocity $\boldsymbol{u}$ at any integration point $\boldsymbol{x}^{a_p}$ can be evaluated as follows:

$$\boldsymbol{u}^{a_p} = [u^{a_p},\ v^{a_p}]^{\mathrm{T}}, \qquad \boldsymbol{u}^{a_p} = \mathcal{I}(\boldsymbol{u})(\boldsymbol{x}^{a_p}) = \left[\sum_{A_x} u^{A_x}\varphi^{A_x}\left(\boldsymbol{x}^{a_p}\right), \sum_{A_y} u^{A_y}\varphi^{A_y}\left(\boldsymbol{x}^{a_p}\right)\right]^{\mathrm{T}} \tag{23}$$

where

$$\varphi^{A_x}(\boldsymbol{x}) = \varphi(\boldsymbol{x} - \boldsymbol{x}^{A_x}), \qquad \varphi^{A_y}(\boldsymbol{x}) = \varphi(\boldsymbol{x} - \boldsymbol{x}^{A_y}) \tag{24}$$

are interpolating kernel functions centred at fluid cell edges A_x and A_y, defined by the spatial position $\boldsymbol{x}^{A_x}$ and $\boldsymbol{x}^{A_y}$, mid-points of their respective fluid cell edges. For a Cartesian Eulerian mesh, it is convenient to formulate the kernel functions by means of a tensor product expansion as follows,

$$\varphi(\boldsymbol{x}) = \frac{1}{\Delta x \Delta y}\phi\left(\frac{x}{\Delta x}\right)\phi\left(\frac{y}{\Delta y}\right), \qquad \boldsymbol{x} = [x,\ y]^{\mathrm{T}} \tag{25}$$

In above equation (25), ϕ is a continuous function approximating the one dimensional Dirac Delta distribution[7, 8]. Similarly, a virtual velocity field vector $\delta\boldsymbol{u}^s = [\delta u^s\ \delta v^s]^{\mathrm{T}}$ evaluated at a structure particle a_p can also be described as,

$$\delta\boldsymbol{u}^{a_p} = [\delta u^{a_p},\ \delta v^{a_p}]^{\mathrm{T}} = \mathcal{I}(\delta\boldsymbol{u})(\boldsymbol{x}^{a_p}) = \left[\sum_{A_x} \delta u^{A_x}\varphi^{A_x}\left(\boldsymbol{x}^{a_p}\right), \sum_{A_y} \delta u^{A_y}\varphi^{A_y}\left(\boldsymbol{x}^{a_p}\right)\right]^{\mathrm{T}} \tag{26}$$

where a consistent interpolating methodology is employed as in equation (23), to ensure conservation of the overall scheme. The internal virtual work formulated in the case of the immersed solid domain is defined as the directional derivative of the Helmholtz's free energy functional with respect to a virtual velocity field vector[9, 10] as follows,

$$\delta W^s_{int}(\boldsymbol{\phi}, \delta\boldsymbol{u}^s) = D\Pi^s(\boldsymbol{\phi})\left[\delta\boldsymbol{u}^s\right] \tag{27}$$

and after substitution of equation (22) into (27), we arrive at

$$\delta W^s_{int}(\boldsymbol{\phi}, \delta\boldsymbol{u}^s) = \int_{\Omega_0^s} \frac{\partial\widehat{\Psi}^s}{\partial\boldsymbol{F}} : D\boldsymbol{F}[\delta\boldsymbol{u}^s]\, dV \simeq \sum_{a_p} W^{a_p}\left(\frac{\partial\widehat{\Psi}^s}{\partial\boldsymbol{F}} : D\boldsymbol{F}[\delta\boldsymbol{u}^s]\right)^{a_p} \tag{28}$$

Alternatively, after a suitable push forward operation, the above formulae (28) can be re-expressed according to an Updated Lagrangian Formulation (ULF) by introduction of the Kirchhoff stress tensor $\boldsymbol{\tau}'^s$ as,

$$\delta W^s_{int}(\boldsymbol{\phi}, \delta \boldsymbol{u}^s) = \int_{\Omega^s_0} \boldsymbol{\tau}'^s : \boldsymbol{\nabla} \delta \boldsymbol{u}^s \, dV \simeq \sum_{a_p} W^{a_p} \boldsymbol{\tau}'^{s,a_p} : \boldsymbol{\nabla} \delta \boldsymbol{u}^{a_p} \tag{29}$$

The evaluation of the above formula (29) requires the computation of the spatial gradient of the virtual velocity at integration point a_p as,

$$\boldsymbol{\nabla} \delta \boldsymbol{u}^{a_p} = \boldsymbol{\nabla} \mathcal{I}(\delta \boldsymbol{u})(\boldsymbol{x}^{a_p}) = \left[\sum_{A_x} \delta u^{A_x} \boldsymbol{\nabla} \varphi^{A_x}(\boldsymbol{x}^{a_p}) \, , \sum_{A_y} \delta v^{A_y} \boldsymbol{\nabla} \varphi^{A_y}(\boldsymbol{x}^{a_p}) \right]^{\mathrm{T}} \tag{30}$$

After re-writing the Kirchhoff stress tensor in the form $\boldsymbol{\tau}'^s = \left[\boldsymbol{\tau}'^s_x, \, \boldsymbol{\tau}'^s_y \right]^{\mathrm{T}}$, equation (29) can be reformulated in a continuum manner as,

$$\delta W^s_{int}(\boldsymbol{\phi}, \delta \boldsymbol{u}^s) = \int_{\Omega^s_0} \left(\boldsymbol{\tau}'^s_x \cdot \boldsymbol{\nabla} \mathcal{I}(\delta u)(\boldsymbol{x}^s) + \boldsymbol{\tau}'^s_y \cdot \boldsymbol{\nabla} \mathcal{I}(\delta v)(\boldsymbol{x}^s) \right) \, dV \tag{31}$$

Substitution of equation (30) back into (31) yields in a discrete manner,

$$\delta W^s_{int}(\boldsymbol{\phi}, \delta \boldsymbol{u}^s) \simeq \sum_{a_p} W^{a_p} \left(\sum_{A_x} \delta u^{A_x} \boldsymbol{\tau}'^{s,a_p}_x \cdot \boldsymbol{\nabla} \varphi^{A_x}(\boldsymbol{x}^{a_p}) + \sum_{A_y} \delta v^{A_y} \boldsymbol{\tau}'^{s,a_p}_y \cdot \boldsymbol{\nabla} \varphi^{A_y}(\boldsymbol{x}^{a_p}) \right) \tag{32}$$

where after interchanging the summation operators, a final re-arrangement of the above formula (32) yields,

$$\delta W^s_{int}(\boldsymbol{\phi}, \delta \boldsymbol{u}^s) = \sum_{A_x} \delta u^{A_x} f^{A_x}_x + \sum_{A_y} \delta v^{A_y} f^{A_y}_y \tag{33}$$

where,

$$f^{A_x}_x = \int_{\Omega^s_0} \boldsymbol{\tau}'^s_x \cdot \boldsymbol{\nabla} \varphi^{A_x}(\boldsymbol{x}^s) dV \simeq \sum_{a_p} W^{a_p} \boldsymbol{\tau}'^{s,a_p}_x \cdot \boldsymbol{\nabla} \varphi^{A_x}(\boldsymbol{x}^{a_p}) \tag{34}$$

$$f^{A_y}_y = \int_{\Omega^s_0} \boldsymbol{\tau}'^s_y \cdot \boldsymbol{\nabla} \varphi^{A_y}(\boldsymbol{x}^s) dV \simeq \sum_{a_p} W^{a_p} \boldsymbol{\tau}'^{s,a_p}_y \cdot \boldsymbol{\nabla} \varphi^{A_y}(\boldsymbol{x}^{a_p}) \tag{35}$$

In order to guarantee conservation of the scheme, and after observing equations (11-12,16-17) and (33), it can be deduced that:

$$g^{A_x}_x = \frac{f^{A_x}_x}{\Omega_{u^{A_x}}}, \qquad g^{A_y}_y = \frac{f^{A_y}_y}{\Omega_{v^{A_y}}} \tag{36}$$

where $g^{A_x}_x$ and $g^{A_y}_y$ represent the fluid-structure interaction force per unit of volume which must be applied at the fluid cell edges A_x and A_y, respectively.

4 Algorithmic comparison of the Immersed Structural Potential Method (ISPM) with alternative immersed methodologies.

In alternative immersed methodologies[11], the deformable solid is modelled using a Finite Element (F.E.) mesh. This way, an interpolation-spreading strategy based upon kernel functions is established exclusively between the background Eulerian fluid cell edges and the immersed nodes of the F.E. solid mesh. The deformation gradient tensor $\boldsymbol{F}$ is then obtained within the immersed continuum by using standard space-varying F.E. shape functions. Equivalent internal forces are computed at the nodes of the F.E. mesh after suitable numerical integration of the stress tensor evaluated at Gauss points. The equivalent nodal forces are then spread back to the Eulerian fluid mesh by means of kernel functions ensuring conservation of the scheme.

Two flowcharts are displayed in Figures (1-2) to explain the various computational steps needed in both the ISPM and by using an alternative immersed methodology, respectively. In both algorithms, for the sake of simplicity, a fixed point iteration scheme is used to guarantee full coupling between the fluid phase and the solid phase within each time step. A residual norm is computed between the two latest available force terms at iterations k and $k+1$, whereby satisfaction of the coupling between both phases is assessed, leading to either a new iteration $k+2$ or a new time step $n+2$.

The number of steps shown in Figure 2 required to complete the calculation of immersed forces $\{f_x^{A_x},\ f_y^{A_y}\}$ is clearly greater than in Figure 1, which results into a more expensive computational algorithm. Specifically, the evaluation of the deformation gradient tensor $\boldsymbol{F}$ at every Gauss point g_p requires two interpolation stages; first, interpolation of the velocity field $\{u^{A_x},\ v^{A_y}\}$ from the fluid mesh to the solid F.E. nodes $\boldsymbol{v}^a$ and, second, computation of $\boldsymbol{F}^{g_p}$ by using the gradient of the F.E. shape functions $\boldsymbol{\nabla}_0 N^a_{g_p}$. Similarly, the computation of the immersed forces $\{f_x^{A_x},\ f_y^{A_y}\}$ at every fluid cell edge is carried out after two spatial integration steps; first, the deviatoric Kirchhoff stress tensor is integrated at every gauss point $\boldsymbol{\tau}'^{g_p}$ to obtain equivalent internal F.E. nodal forces $\boldsymbol{f}^a$ and, second, the forces are then spread to the fluid cell edges. Furthermore, looping over elements and over gauss points in turn, is more computationally demanding than looping over integration points.

- Fixed point iteration, while $\|\boldsymbol{f}_k^{n+1} - \boldsymbol{f}_{k-1}^{n+1}\|/\|\boldsymbol{f}^n\| > tolerance$
  - Compute solid immersed forces
    - Loop over integration points a_p
      1. Interpolate velocity field at structure integration points a_p

$$\boldsymbol{u}_{k+1}^{a_p,n+1} = \mathcal{I}\left(\boldsymbol{u}_{k+1}^{n+1}\right)\left(\boldsymbol{x}_k^{a_p,n+1}\right)$$

      2. Interpolate velocity gradient tensor at structure integration points a_p

$$\boldsymbol{l}_{k+1}^{a_p,n+1} = \left[\boldsymbol{\nabla}\mathcal{I}\left(\boldsymbol{u}_{k+1}^{n+1}\right)\left(\boldsymbol{x}_k^{a_p,n+1}\right)\right]$$

      3. Integrate $\dot{\boldsymbol{F}} = \boldsymbol{l}\boldsymbol{F}$ according to

$$\boldsymbol{F}_{k+1}^{a_p,n+1} = e^{\left(\Delta t \boldsymbol{l}_{k+1}^{a_p,n+1}\right)}\boldsymbol{F}^{a_p,n}$$

      4. Evaluate constitutive law to obtain deviatoric Kirchhoff stress

$$\boldsymbol{\tau}_{k+1}^{\prime s,a_p,n+1} = \mathcal{G}(\boldsymbol{F}_{k+1}^{a_p,n+1}, \boldsymbol{l}_{k+1}^{a_p,n+1})$$

      5. Spatial integration of Kirchhoff stress to obtain forces at fluid cell edges

$$f_{i,k+1}^{A_i,n+1} = \sum_{a_p} W^{a_p}\boldsymbol{\tau}_i^{\prime s,a_p} \cdot \boldsymbol{\nabla}\varphi^{A_i}(\boldsymbol{x}^{a_p}), \quad i = x, y$$

      6. Add inertia and gravity forces if required at fluid cell edges

$$f_{i,k+1}^{ine,A_i,n+1} = \sum_{a_p} W^{a_p}\Delta\rho^{a_p}\left(g_i - \left.\frac{D(\boldsymbol{u}^{a_p}\cdot\boldsymbol{e}_i)}{Dt}\right|_{k+1}^{n+1}\right)\varphi^{A_i}\left(\boldsymbol{x}_k^{a_p,n+1}\right)$$

      7. Update spatial position of integration points a_p

$$\boldsymbol{x}_{k+1}^{a_p,n+1} = \boldsymbol{x}^{a_p,n} + \frac{1}{2}\Delta t\left(\boldsymbol{u}_{k+1}^{a_p,n+1} + \boldsymbol{u}^{a_p,n}\right)$$

  - Solve Navier-Stokes equations to obtain p_{k+2}^{n+1}, $u_{k+1}^{A_x,n+1}$, $v_{k+1}^{A_y,n+1}$

Figure 1: Flowchart of the Immersed Structural Potential Method .

- Fixed point iteration, while $\|\boldsymbol{f}_k^{n+1} - \boldsymbol{f}_{k-1}^{n+1}\|/\|\boldsymbol{f}^n\| > tolerance$
  - Compute solid immersed forces
    1. Interpolate velocity field at F.E. mesh nodes a:
$$\boldsymbol{u}_{k+1}^{a,n+1} = \mathcal{I}\left(\boldsymbol{u}_{k+1}^{n+1}\right)\left(\boldsymbol{x}_k^{a,n+1}\right)$$
    2. Time integration of the spatial position for node a:
$$\boldsymbol{x}_{k+1}^{a,n+1} = \boldsymbol{x}^{a,n} + \frac{1}{2}\left(\boldsymbol{u}_{k+1}^{a,n+1} + \boldsymbol{u}^{a,n}\right)$$
    3. Loop over elements e
       · Loop over Gauss points g_p for element e
       i. Compute deformation gradient $\boldsymbol{F}$ at Gauss point g_p:
$$\boldsymbol{F}_{k+1}^{g_p,n+1} = \sum_a \boldsymbol{x}_{k+1}^{a,n+1} \otimes \boldsymbol{\nabla}_0 N_{g_p}^a$$
       ii. Compute velocity gradient $\boldsymbol{l}$ at Gauss point g_p:
$$\boldsymbol{l}_{k+1}^{g_p,n+1} = \sum_a \boldsymbol{u}_{k+1}^{a,n+1} \otimes \boldsymbol{\nabla} N_{g_p}^a$$
       iii. Evaluate constitutive law to obtain deviatoric Kirchhoff stress:
$$\boldsymbol{\tau}'^{s,g_p,n+1}_{k+1} = \mathcal{G}(\boldsymbol{F}_{k+1}^{g_p,n+1}, \boldsymbol{l}_{k+1}^{g_p,n+1})$$
       iv. Spatial integration of Kirchhoff stress to obtain forces at each node a:
$$\boldsymbol{f}_{k+1}^{a,n+1} = \sum_{g_p} J^{g_p} \boldsymbol{\tau}'^{s,g_p} \boldsymbol{\nabla} N_{g_p}^a$$
       v. Add inertia and gravity forces if required at each node a:
$$\boldsymbol{f}_{k+1}^{ine,a,n+1} = \sum_{g_p} J^{g_p} \Delta\rho^{g_p} \left(\boldsymbol{g} - \sum_b N_{g_p}^a N_{g_p}^b \frac{D}{Dt}\left(\boldsymbol{u}_{k+1}^{a,n+1}\right)\right)$$
    4. Spread nodal forces back onto the fluid cell edges:
$$f_i^{A_y} = \mathcal{S}_i(\boldsymbol{f})(\boldsymbol{x}^{A_y}), \quad i = x, y$$
  - Solve Navier-Stokes equations to obtain p_{k+2}^{n+1}, $u_{k+1}^{A_x,n+1}$, $v_{k+1}^{A_y,n+1}$

Figure 2: Flowchart of alternative immersed methodology.

5 NUMERICAL EXAMPLES

In this section we present some examples featuring the interaction of membranes with a range of flows. The purpose of this will be to show via examples some of the qualities of the numerical solution that is attained with the ISPM.

5.1 Two dimensional membrane under constant amplitude Poiseuille flow

For the first case, we will consider the interaction of a two dimensional membrane with a constant amplitude Poiseuille flow in a rectangular channel. This can serve as an idealisation of a two dimensional blood vessel (see Figure 3). As a first approximation, we will consider it to be filled with an incompressible Newtonian viscous fluid with viscosity $\mu = 10$ dyne/cm^2 and density $\rho = 100$g/cm^3. Both top and bottom boundaries are treated as walls (non-slip) and are fixed, and a thin flexible membrane is attached to the top wall. A Poiseuille inlet condition with constant amplitude $A(t) = 1$ cm/s is applied on the left hand side of the domain ($x = 0$) and outflow boundary conditions are applied on the right side. The membrane considered will be initially rectangular of 0.0212 cm in width and 0.8 cm in length, and its constitutive behaviour will be assumed to be that of a nearly incompressible Neo-Hookean material, with shear modulus $\mu_s = 2 \cdot 10^7$dyne/cm^2 and the same density than that of the surrounding fluid.

This problem has been solved with both the EIBM and the ISPM in time, and as it is to be expected, the flexible membrane deforms under the force exerted by the fluid (see Figure 4) and consequently distorts the corresponding flow. It is particularly worth turning our attention to a particular feature of the solution: the satisfaction of the incompressibility constraint. In Figure 5 we can observe the Jacobian of the deformation gradient for both EIBM and ISPM at time $t = 3$ s. As it can be seen in the corresponding solution obtained using the EIBM, errors in J are in the range of -35% to 25% approximately. These excessive errors are localised around the root tip, leading edge and flap tips. It can be shown that faster flows (hence causing more deformation) can even produce negative Jacobians in some elements, halting execution. If we look now at the corresponding solution using the ISPM (Figure 5b), the corresponding J is 1 throughout the structure. This is due to the structure-preserving scheme employed in the ISPM to obtain the deformation gradient tensor after time integration of the spatial velocity gradient tensor. It is worth noting that this is a very important feature to preserve in this type of problems, as not doing so quickly leads to unacceptable errors, and eventually, non-robustness of the algorithm.

In previous sections it has been shown how the ISPM is less computationally demanding by merely comparing the number of interpolations and way in which forces are integrated. We can also show this in a much more tangible way by means of runtime comparisons per number of integration points/mesh nodes used to discretise the solid. In Figure 6 it can be observed that alternative immersed methodologies (EIBM) are from 23% to 26% more expensive than the equivalent discretisation using ISPM.

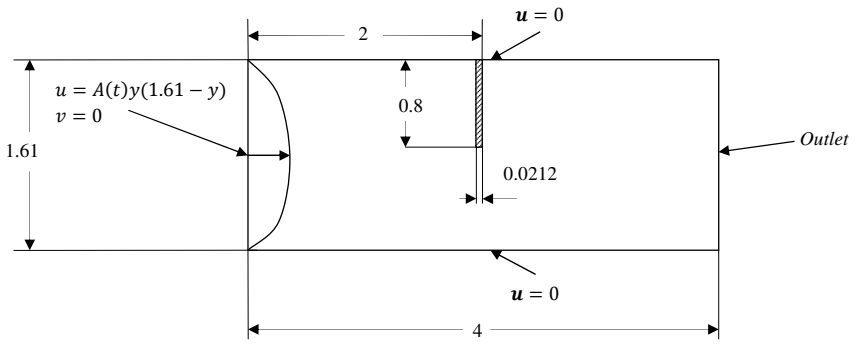

Figure 3: Geometry and boundary conditions for a flexible membrane subjected to steady Poiseuille flow (not drawn to scale). Dimensions are in cm.

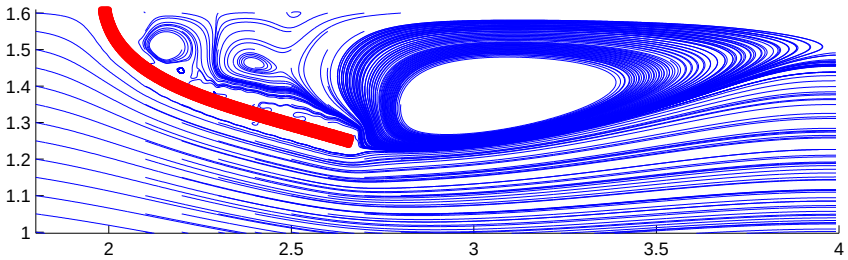

Figure 4: Streamlines (in blue) and membrane position for $t = 3$ s using the ISPM.

5.2 Three dimensional membrane subjected to pulsatile flow

In this section we consider a generalisation of the above example to a thin elastic membrane immersed in a fully three dimensional viscous fluid with viscosity $\mu = 1$ dyne/cm^2 and density $\rho = 1$ g/cm^3. For simplicity, we initially consider a prismatic channel Ω of 8 cm in length and 2 cm in height and depth and place a nearly incompressible Neo-hookean ($\mu_s = 3846$ dyne/cm^2, $\rho = 1$ g/cm^3) flat membrane Ω_s of dimensions $0.02 \times 1 \times 2$ cm occluding half of the channel. The geometry can be seen as a simple extrusion of the previous two dimensional flap example, with the subtle difference of the boundary conditions. We will consider a tensor product of a Poiseuille flow for the inlet on the left and outlet boundary conditions on the right. All the other boundaries will be treated as non-slip walls. Please note that this attaches the membrane not only to the top of the channel, but also to the frontal and rear walls, creating a clearly different problem than that modelled by the two dimensional counterparts. We also consider an inlet flow pulsatile in amplitude modulated by

$$A(t) = \frac{5}{2}\left(\sin\left(2\pi t\right) + 1.1\right) \tag{37}$$

We discretise the fluid in a sequence of meshes with $(2^{4+i}, 2^{2+i}, 2^{2+i})$ cells in x-,y- and z-directions for $i = 1, \ldots, 3$, and the solid using 18865, 46900 and 125265 integration nodes respectively. In Figure 7 three different snapshots of the solution can be observed for

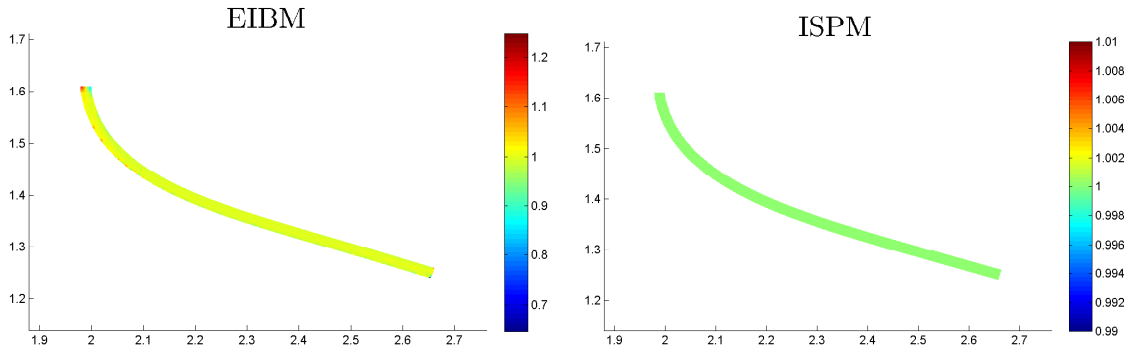

Figure 5: Jacobian of the deformation gradient F for the deformable membrane under Poiseuille flow for $t = 3$ s: (a) EIBM; (b) ISPM. Dimensions are in cm.

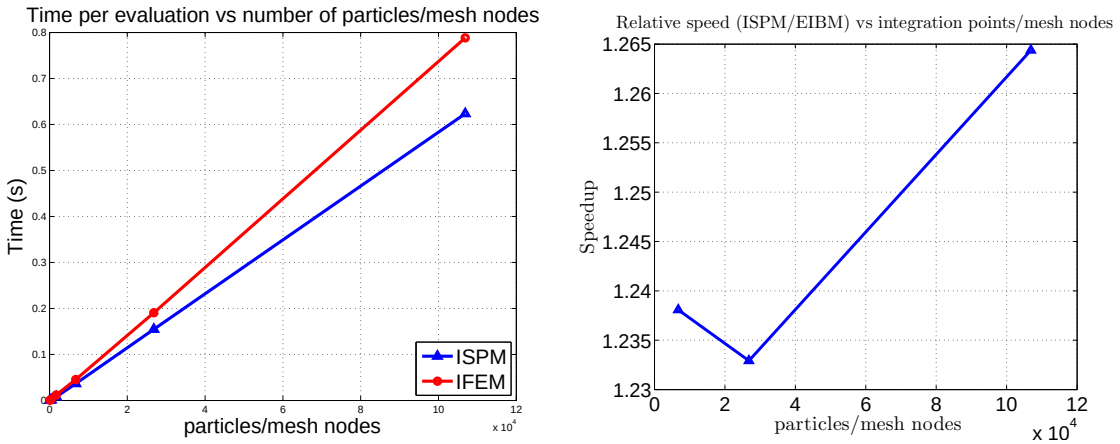

Figure 6: Left: Time (s) required to evaluate FSI forces vs. number of integration points (ISPM) / FE mesh nodes (EIBM). Right: Relative speedup of ISPM vs EIBM as a function of number of integration points (computed as the ratio of time required by EIBM / time required by ISPM).

$i = 3$. As it can be seen in the figure, the method successfully captures the flow pattern created by the presence of the membrane. Up to time $t = 0.25$ s the flow is accelerating thus stretching the membrane towards the right. As it decelerates (for times between $t = 0.25$ s and $t = 0.5$ s) a complex vortex forms downstream of the membrane that causes it to bend and fold slightly.

6 CONCLUSIONS

In this paper, the new Immersed Structural Potential Method has been revisited and formulated following an integral formulation. Specifically, the incompressible Navier-Stokes fluid equations have been resolved according to a low order Finite Volume staggered formulation and the force field source term, characteristic of any immersed methodology, has been introduced following variational principles. Conservation of the scheme is guar-

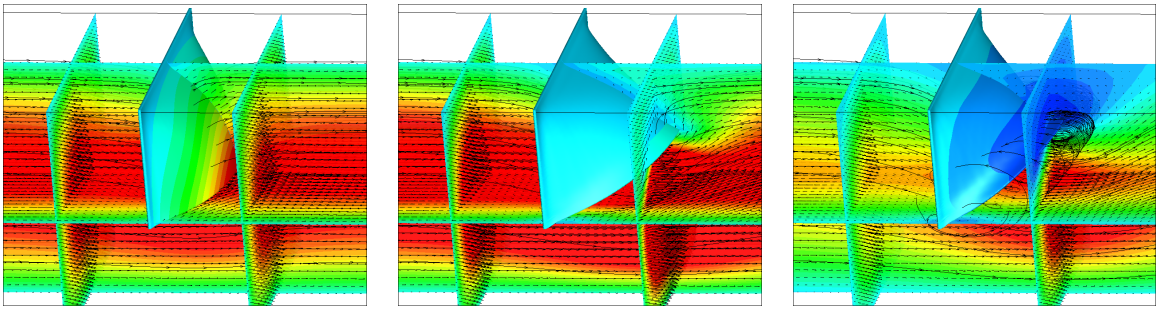

$t = 0.15$ s $\qquad$ $t = 0.3$ s $\qquad$ $t = 0.5$ s

Figure 7: Streamlines, velocity slices and deformation of a thin elastic leaflet under 3D pulsatile flow. Colour represents horizontal velocity component.

anteed due its construction and satisfaction of the incompressibility constraint is also fulfilled as a result of the suitable time integration of the spatial velocity gradient tensor. The methodology described compares very well with existing immersed methodologies in terms of accuracy and displays a dramatic improvement with respect to inadmissible changes in volume. Furthermore, it provides a substantial saving in computational time as well as greater algorithmic simplicity, making it very attractive for subsequent implementation into parallel architecture.

REFERENCES

[1] A. J. Gil, A. Arranz Carreño, J. Bonet, and O. Hassan. The Immersed Structural Potential Method for haemodynamic applications. *Journal of Computational Physics*, accepted for publication, 2010.

[2] C. S. Peskin. Flow patterns around heart values: a numerical method. *Journal of Computational Physics*, 10:252–271, 1972.

[3] W. K. Liu, Y. Liu, D. Farrell, L. Zhang, X. S. Wang, Y. Fukui, N. Patankar, Y. Zhang, C. Bajaj, J. Lee, J. Hong, X. Chen, and H. Hsu. Immersed finite element method and its applications to biological systems. *Computer Methods in Applied Mechanics and Engineering*, 195:1722–1749, 2006.

[4] D. Sulsky, Z. Chen, and H. L. Schreyer. A particle method for history-dependent materials. *Computer Methods in Applied Mechanics and Engineering*, 118(1-2):179 – 196, 1994.

[5] A. R. York II, D. Sulsky, and H. L. Schreyer. Fluid-membrane interaction based on the material point method. *International Journal for Numerical Methods in Engineering*, 48(6):901–924, 2000.

[6] F. H. Harlow and J. E. Welch. Numerical calculation of time-dependent viscous incompressible flow of fluid with free interface. *The Physics of Fluids*, 8:2182–2189, 1965.

[7] C. S. Peskin. The immersed boundary method. *Acta Numerica*, 11(479-517), 2002.

[8] A. M. Roma, C. S. Peskin, and M. J. Berger. An Adaptive Version of the Immersed Boundary Method. *Journal of Computational Physics*, 153(2):509 – 534, 1999.

[9] G. A. Holzapfel. *Nonlinear solid mechanics*. Wiley, 2000.

[10] J. Bonet and R. D. Wood. *Nonlinear continuum mechanics for finite element analysis*. Cambridge University Press, second edition edition, 2008.

[11] X. Wang and W. K. Liu. Extended immersed boundary method using FEM and RKPM. *Computer Methods in Applied Mechanics and Engineering*, 193(12-14):1305–1321, 2004. Meshfree Methods: Recent Advances and New Applications.